A Comprehensive Methodology to Assess Tropospheric Fade Affecting Earth-Space Communication Systems

Lorenzo Luini, *Senior Member, IEEE*

***Abstract*— ATM PROP (ATMospheric simulator for PROPagation applications), a comprehensive methodology to assess tropospheric effects affecting high-frequency Earth-space communication systems, is presented. The model takes advantage of physically-based approaches aimed at synthesizing high-resolution (1 km×1 km horizontal, 100 m vertical) three-dimensional fields of rain, clouds and water vapor (dimension: 200 km× 200 km horizontal, 20 km vertical), which are all merged so as to maintain their mutual correlation. This, in turn, enables a more realistic combination of the attenuation due to single constituents, if compared to the statistical approach currently recommended by the ITU-R. The accuracy of ATM PROP in predicting tropospheric effects on Earth-space systems is initially validated against the large propagation dataset collected at the experimental station of Spino d'Adda, Italy, during the ITALSAT propagation campaign. The preliminary results obtained suggest that ATM PROP can be used to predict, with a reasonable level of complexity and limited coarse-resolution NWP-derived inputs, the tropospheric fade affecting complex communication systems (e.g. site diversity schemes), especially those involving low elevation links (e.g. LEO or GEO at high latitude), for which the spatial distribution of the relevant tropospheric constituents needs to be taken in due account.**

***Index Terms*— Electromagnetic wave propagation, atmospheric effects, satellite communications.**

I. Introduction

THE operational frequency of modern satellite communication (SatCom) systems is gradually shifting to the spectrum portion above the traditional Ku band, in order to take advantage of the larger bandwidths available, as well as to avoid channel congestion and interference issues. This is the case of satellites already operating in the Ka band (e.g. Ka-SAT in Europe and DirectTV-12 in the USA, as for geostationary satellites, and the O3b fleet, as for Medium Earth Orbit satellites) and of Smart Gateways, which are foreseen to upload contents with carriers in the Q/V band [1]. Recently, interest has also arisen in SatCom systems planned to operate even at higher frequencies, namely in the W band [2], [3]. The same increase in the operational frequency is also taking place in Earth Observation (EO) systems (shift from the X band to the Ka band) because of the need of larger bandwidths required to download at high symbol rates the always increasing amounts of data from EO satellites to ground stations [4].

As is well known, the main drawback to the use of higher frequencies comes from atmospheric constituents, namely gases, clouds and hydrometeors, which cause extinction (absorption and scattering) of the radiated electromagnetic (EM) power [5]. Detrimental effects increase significantly with frequency and, accordingly, the availability and Quality of Service (QoS) of SatCom systems become progressively more critical [3]. As a result, significant research activities have been promoted so far for the in-depth investigation of such impairments to electromagnetic waves propagating in the atmosphere. This includes propagation experiments such as those involving the ATS, COMSTAR and ACTS satellites in the USA, and the SIRIO, OLYMPUS, ITALSAT and Alphasat satellites in Europe.

Besides experiments, also theoretical research activities have been promoted (e.g. [2], [6]), mainly with the goal of developing models for the prediction of propagation impairments, as well as for the simulation and performance evaluation of complex systems implementing Fade Mitigation Techniques (FMTs) [7]. These investigations assume even higher significance when very high frequencies are addressed, such as the V and W bands, because, as no or scarce experimental data are available, in this case, only models can be used for system design [3]. As a result, with the increase in frequency, prediction models are requested to be not only more and more accurate and reliable, but also flexible enough to be adapted to different scenarios. This has pushed the recent tendency in theoretical research activities to move from empirical models, typically developed on the basis of experimental data and valid only in specific climatic regions and/or frequency ranges, to physically-based methodologies which inherently aim at being globally applicable as well as reliable also outside the range of frequencies in which they have been developed/tested. This is the case of complex approaches aimed at reproducing the atmospheric environment

Manuscript received XXXX.

Lorenzo Luini is with the Dipartimento di Elettronica, Informazione e Bioingegneria, Politecnico di Milano, Piazza Leonardo da Vinci, 32, 20133, Milano, Italy, and with the Istituto di Elettronica e di Ingegneria dell'Informazione e delle Telecomunicazioni (IEIIT), Consiglio Nazionale delle Ricerche, Via Ponzio 34/5, Milano 20133, Italy (e-mail: lorenzo.luini@polimi.it).

affecting the propagation of EM waves, from which the performance of any wireless system can be afterwards predicted. Some of these methodologies are inherently limited as they consider only single constituents (see e.g. [8]-[12] for rain, [13] and [14] for clouds, and [15] for water vapor), while others (see e.g. [16] and [17]), typically relying on outputs of meteorological Limited Area Models, generate the full tropospheric environment, though at the expense of a very high level of complexity and of long and heavy computations.

Moving along this track, this contribution presents ATM PROP (ATMospheric simulator for PROPagation applications), a comprehensive methodology offering a compromise between completeness and complexity in reproducing the tropospheric environment and its effects on EM waves: indeed ATM PROP takes into account only those meteorological fields really required to estimate full tropospheric attenuation, thus minimizing the complexity and computation effort, yet delivering a high degree of prediction accuracy. More specifically, this goal is achieved by merging MultiEXCELL [8], SMOC [13] and SMOV [15], methodologies that synthesize high resolution (1 km×1 km horizontal, 100 m vertical) three-dimensional fields of rain, clouds and water vapor (dimension: 200 km× 200 km horizontal, 20 km vertical), starting from few coarse-resolution NWP-derived inputs. Such fields are properly merged to maintain their mutual correlation: as a result, ATM PROP not only enables a more realistic combination of the attenuation due to single constituents (range: 20-100 GHz), if compared to the statistical approach currently recommended by the ITU-R, but it is also suitable to consider critical communication systems involving e.g. LEO links or GEO links at high latitude, for which the spatial distribution of the relevant tropospheric constituents needs to be taken in due account to yield more accurate predictions.

The remainder of the paper is structured as follows: Section II describes how rain fields and cloud fields generated by MultiEXCELL and SMOC, respectively, are properly combined, while Section III presents how the gaseous components affecting the propagation of EM waves (water vapor and oxygen) are included into ATM PROP. Section IV deals with the calculation of the total tropospheric attenuation using ATM PROP, while Section V offers its validation by comparing the attenuation statistics estimated using ATM PROP against the data collected during the ITALSAT propagation campaign at the experimental station of Spino d'Adda. Finally, Section VI draws some conclusions.

II. Precipitation and Clouds

A. MultiEXCELL

Presented in [8], MultiEXCELL (Multi EXPonential CELL) is a global rainfall model oriented to the investigation and prediction of atmospheric electromagnetic wave propagation impairments. MultiEXCELL generates sets of synthetic rain fields, whose ensemble preserves the local rainfall statistics (the only input to the model) and reproduces the correct rainfall spatial correlation.

Square synthetic rain fields, whose spatial resolution is 1 km×1 km and whose lateral dimension can range between 200 and 300 km, result from the arrangement of multiple synthetic exponential cells according to the natural rain cells' aggregative process observed in radar-derived precipitation maps. Moreover, MultiEXCELL reproduces the statistical distribution of the fractional rainy area, in turn estimated from the rain amount accumulated in 6-hour slots, M_t, extracted from the ECMWF (European Centre for Medium-range Weather Forecast) ERA40 database [18]. A key advantage of MultiEXCELL is that a relatively small set of synthetic rain fields (around 400/500 maps) is sufficient to reliably represent the local rainfall process and, thus, to efficiently simulate the interaction between precipitation and wireless telecommunication systems [19],[20].

As an additional feature improving MultiEXCELL, synthetic rain maps can be classified as stratiform or convective on the basis of the peak rain rate discrimination value $R_{M,th}$ introduced in [21], which, in turn, is tightly linked to the local rain rate Complementary Cumulative Distribution Function (CCDF) − typically referred to as $P(R)$ − the only input to MultiEXCELL [8]. Specifically, a rain map is classified as stratiform if its peak rain rate is lower than $R_{M,th}$, and as convective if the rain intensity associated to at least one pixel in the map exceeds $R_{M,th}$. As an example, Fig. 1 depicts the stratiform, convective and total rain $P(R)$s, calculated from the classified MultiEXCELL rain maps generated for Spino d'Adda, Italy (latitude 45.4° N and longitude 9.5° E, 81 m a.m.s.l.), for which, according to [21], $R_{M,th}$ = 15 mm/h. As discussed in [22], the discrimination into different precipitation types is beneficial because it allows to more accurately take into account the different effects of stratiform and convective rain on Earth-space links (e.g. different rain height and presence of the melting layer only during stratiform events).

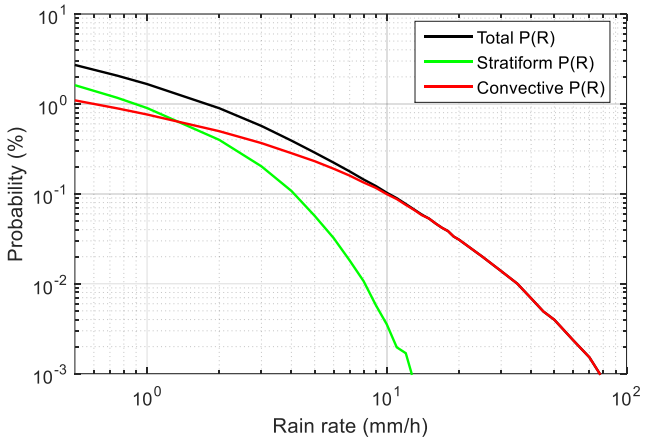

Fig. 1. Stratiform, convective and total $P(R)$s obtained from the classified MultiEXCELL rain maps; results for Spino d'Adda, Italy.

B. SMOC

Introduced in [13], SMOC (Stochastic MOdel of Clouds) is a methodology to generate the three-dimensional distribution

of the liquid water content w with high resolution (1 km×1 km horizontal, 100 m vertical) across areas as large as 200 km×200 km, starting from coarse integral information on clouds typically available as part of global gridded NWP (Numerical Weather Prediction) products. This is achieved by exploiting features observed in real cloud fields (MODIS and CloudSat data), and from the knowledge of the fractional cloud cover (f_C) and of the average integrated cloud liquid water content (L_C), both associated with a large NWP pixel of dimension 2°×2° (latitude×longitude). Specifically, SMOC relies on the ERA40 database to derive the necessary inputs (referred to as f_{ERA} and L_{ERA}). More details on the rationale and features of SMOC are reported in [13], which also shows that the generated cloud fields reflect the spatial correlation of w observed in real cloud fields and reproduce with good accuracy the local statistics of the integrated liquid water content.

C. Combination of MultiEXCELL and SMOC

The proper combination of the synthetic fields generated by MultiEXCELL and SMOC must reflect the correlation existing between the rain rate R and the integrated liquid water content L, and, at the same time, the two models need to correctly reproduce the main features of R and L, i.e. their first- and second-order statistics. As mentioned in [8] and in [13], both MultiEXCELL and SMOC receive as input coarse meteorological data extracted from the ERA40 database (M_t for MultiEXCELL, L_{ERA} and f_{ERA} for SMOC); notwithstanding this, the synthesis of rain and cloud fields relies on markedly different approaches: indeed, MultiEXCELL combines multiple synthetic rain cells with deterministic (exponential) shape to preserve the occurrence and the spatial distribution of precipitation [8], while SMOC relies on a more marked stochastic approach [23]. As a result, the combination of rain rate and cloud fields, not at all a straightforward task, requires some care and can be achieved according to the following guidelines.

1) Rain field generation with MultiEXCELL

For a given site, MultiEXCELL is applied according to the procedure described in [8] to synthesize 400/500 rain fields, starting from the ERA40-derived probability density function (PDF) of M_t (10 years of data) and from the local $P(R)$ (point rain rate statistics with 1-minute integration time).

2) Generation of cloud fields matching rain fields

For each rain map, a cloud field is generated with the obvious constraints that the fractional cloud cover f_C is larger than the fractional rainy area f_R and that all rainy pixels are covered by clouds. As a result, a suitable couple of f_{ERA} and L_{ERA}, satisfying the constraint $f_{ERA} > f_R$, is extracted from the associated PDFs, obtained from at least 5 years of f_{ERA} and L_{ERA} values.

In addition, while synthesizing the cloud field, a simple pattern matching algorithm is implemented to ensure that, as it is physically the case, precipitation originates from heavier clouds. In order to achieve this, making reference to [23], the initial Gaussian field $g(x,y)$ required to synthesize the cloud field is generated with a lateral dimension that is much larger than the one of the rain field. This allows searching for the area of this large $g(x,y)$ map resembling more the rain rate pattern of the target MultiEXCELL rain field; from the practical point of view, this goal is achieved by calculating the two-dimensional cross correlation C_{RC} between the rain field and the large $g(x,y)$, and by identifying the maximum value of C_{RC}. This procedure is exemplified in Fig. 2, which shows the initial large spatially-correlated Gaussian field with dimension 1000 km×1000 km (top side), as well as the area having the highest cross-correlation with the target rain field, the latter being reported in the right-end corner. As is clear by comparing such a field with the final cloud field, besides covering all rainy pixels, clouds are distributed in such a way that the peak value of L (x = 85 km, y = 116 km) falls in the area where the precipitation intensity is higher.

3) Rain height and cloud base

As for the vertical profile, according to MultiEXCELL [8], the rain rate is assumed to be constant from the ground up to the rain height h_R, where the cloud base height is expected to lie. According to the SC EXCELL (Stratiform Convective EXponential CELL) model [22], different rain heights are chosen for stratiform and convective rain maps, so as to reflect the different effects that the two types of precipitation have on Earth-space links. Specifically, according to [24], in which the applicability of SC EXCELL was extended to 85 GHz, stratiform and convective rain heights (H_{str} and H_{cnv}, respectively) are calculated using information on the 0 °C isotherm height, on the stratiform and convective precipitation amounts, and on the 6-hour rainy period probability, all of which are extracted, on monthly basis, from the ERA40 database. Moreover, the convective rain height includes an enhancement factor, which takes into account that during convective events rain particles are typically present also above the 0 °C isotherm height, while the stratiform rain height comprises the (frequency dependent) contribution to attenuation of the bright band. The reader is addressed to [24] for the complete expressions of H_{str} and H_{cnv}.

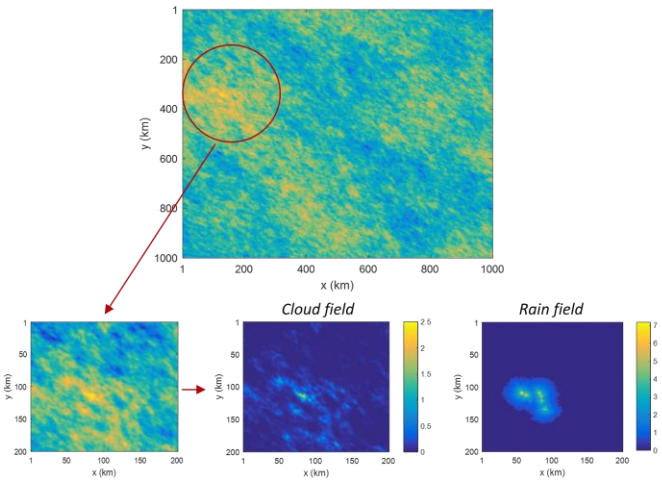

Fig. 2. Example of the combination of a rain field generated by MultiEXCELL (ground rain rate) and of a cloud field (integrated liquid water content) synthesized by SMOC.

4) Rain-free cloud fields

The last step to combine rain and clouds consists in generating a suitable number of rain-free cloud fields to maintain the local yearly probability to have rain ($P_{0,R}$) and to have clouds ($P_{0,C}$), inferred from the local $P(R)$ and from the long-term average value of f_{ERA}, respectively. While completing this last step, having no limitations on the choice of the horizontal extent of clouds necessary to cover the area affected by rain, couples of f_{ERA} and L_{ERA} are randomly extracted with the only constraint to maintain the respective ERA40-derived PDFs. This is goal is achieved with ease because $P_{0,C}$ (e.g. ranging roughly between 40% and 90% in temperate areas) is typically much higher than $P_{0,R}$ (e.g. ranging approximately between 1% and 10% in temperate areas), which implies that the number of rain-free cloud fields largely exceeds the amount of rainy cloud fields. Fig. 3 and Fig. 4 show the final very good agreement between the target PDFs originating from the 5 years of f_{ERA} and L_{ERA} values (the reference site is again Spino d'Adda), as well as from the same values characterizing all the cloud fields generated by SMOC.

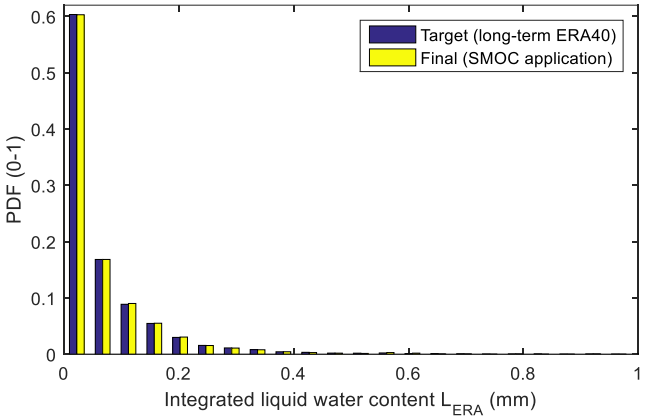

Fig. 3. PDF originating from 5 years of L_{ERA} values extracted from the ERA40 database (the reference site is Spino d'Adda), as well as from the same values characterizing all the cloud fields generated by SMOC.

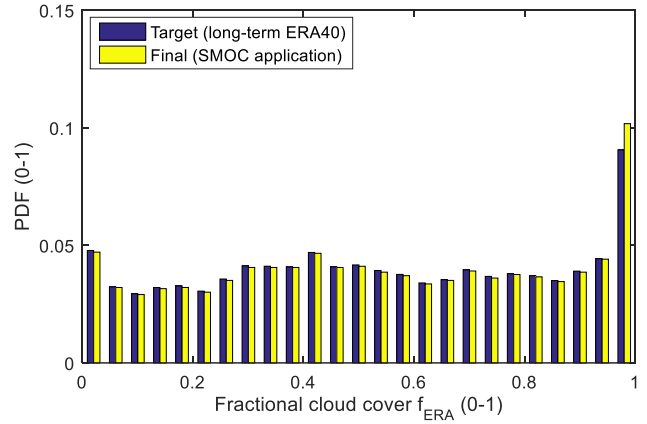

Fig. 4. PDF originating from 5 years of f_{ERA} values extracted from the ERA40 database (the reference site is Spino d'Adda), as well as from the same values characterizing all the cloud fields generated by SMOC.

As a matter of fact, the combination of rain and cloud fields can be achieved because the generation methodology for cloud fields is stochastic and, as such, it is inherently characterized by some degree of randomness that can be advantageously exploited to satisfy the constraints mentioned above. This is also made easier by the fact that the field generation does not follow the time stream of the ERA40 data (which, in other words, would mean to inevitably bind M_t to a couple of f_{ERA} and L_{ERA}), but, as originally devised for MultiEXCELL, the input values to the models are extracted from the respective ERA40-derived PDFs. Besides simplifying the task of combining rain and cloud fields, this approach also allows to use a reduced number of maps to properly reproduce the long-term mean yearly distributions of the rain rate and of the integrated liquid water content for a given location.

III. Gaseous Components

A. Water vapor fields

Recently presented in [15], SMOV (Stochastic MOdel of water Vapor) is a methodology to generate synthetic fields of water vapor concentration v (g/m^3) with 1 km×1 km horizontal resolution and 100 m vertical sampling, from the ground up to 20 km. The model relies on the same stochastic approach underpinning SMOC: the spatial distribution of the integrated water vapor content is generated using as input ERA40 integral values of V, averaged over pixels of dimension 2°×2° (hereinafter referred to as V_{ERA}), and according to the spatial correlation observed in MODIS-derived V fields. As for the vertical profile, v follows the customary exponential decrease with altitude, typically observable from NWP and ROABS (radiosonde observation) data [15].

The integration of SMOV into ATM PROP is achieved by preserving the concurrency among the ERA40 integral values used to generate water vapor fields (V_{ERA}) and cloud fields (f_{ERA} and L_{ERA}). In fact, the synthesis procedure starts from water vapor fields in cloudy conditions: when a couple (f_{ERA}, L_{ERA}) associated to a given 6-hour time slot of the ERA40 database t^* is selected to generate a cloud field (refer to Section II.C), the V_{ERA} value associated to the same ERA40 time slot t^* is used to synthesize the associated water vapor field according to the stochastic procedure outlined in [15]. This approach maintains the high-level correlation between clouds and water vapor, while the small-scale spatial correlation between the two quantities, i.e. the correspondence between L and V pixels with 1 km×1 km spatial resolution, is achieved by applying again the simple pattern matching algorithm described in Section II.C: the goal is indeed to associate the larger values of water vapor to the heaviest clouds, as it should be the case. As an example, Fig. 5 shows a SMOV synthetic water vapor field coupled with a cloud field generated by SMOC: the two fields reflect the soft constraint discussed above as, indeed, higher values of integrated water vapor content cover the area affected by heavier clouds.

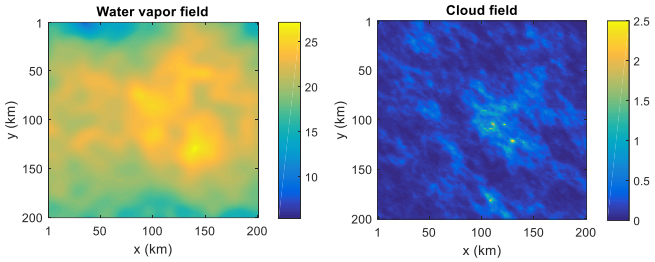

Fig. 5. A sample water vapor field generated by SMOV (left side) associated to a cloud field synthesized by SMOC (right side).

Following the approach used to generate rain-free cloud maps, SMOV water vapor fields in clear sky conditions, given the lack of any constraints, are produced by randomly extracting V_{ERA} values with the aim of maintaining the PDF of V_{ERA} derived from the ERA40 database. The task is easily achieved in this case as well, as depicted in Fig. 6, which compares the statistical distribution of V_{ERA} as calculated from all the ERA40 values and as derived from the V_{ERA} values used to synthesize the water vapor fields for Spino d'Adda: the agreement between the two PDFs is definitely satisfactory.

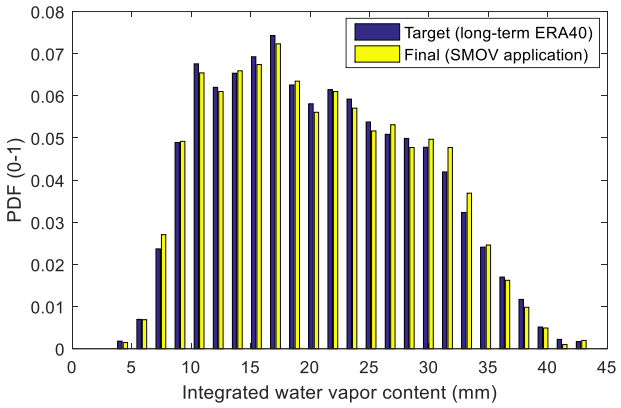

Fig. 6. PDF originating from 5 years of V_{ERA} values extracted from the ERA40 database (the reference site is Spino d'Adda), as well as from the same values characterizing all the water vapor fields generated by SMOV.

B. Contribution of oxygen

Though the impact of oxygen on the propagation of electromagnetic waves is rather limited, apart from absorption peaks (such as the one around 60 GHz), for the sake of completeness, its effect is included in ATM PROP as well. As is clarified in [25], the attenuation due to oxygen depends on pressure P and temperature T: for a very accurate calculation of oxygen attenuation, the full vertical profile of P and T should be available (e.g. from RAOBS data). On the other hand, for a fixed height (e.g. a layer close to the ground), both P and T are rather stable across areas as large as the atmospheric fields considered in ATM PROP, which, in turn, allows to easily calculate the slant path attenuation due to oxygen, A_S^{OX}, from the zenithal attenuation, A_Z^{OX}:

$$A_S^{OX} = A_Z^{OX} / \sin\theta \quad \text{(dB)} \qquad (1)$$

being θ the link elevation angle.

Considering in addition that [25] offers in Annex 2 a simplified yet accurate procedure to estimate A_Z^{OX} from the sole knowledge of the ground pressure and temperature (P_G and T_G, respectively), the impact of oxygen on electromagnetic waves is integrated into ATM PROP only in terms of total path attenuation. In other words, no full three-dimensional fields of oxygen concentration nor of P and T are actually generated, but rather, the information on P_G and T_G is extracted from the ERA40 database (henceforth referred to as P_{ERA} and T_{ERA}, respectively) for the application of the simplified model in [25] aimed at estimating A_Z^{OX} (and A_S^{OX} as well through (1)). Like for V_{ERA}, the concurrency between P_{ERA} and T_{ERA} and the other ERA40 derived quantities (i.e. V_{ERA}, f_{ERA}, L_{ERA}) is preserved: as an example, Fig. 7 shows the good agreement between the PDFs obtained from 5 years of P_{ERA} values included in the ERA40 database and from the same values associated to the water vapor fields generated by SMOV for Spino D'Adda (very similar results, omitted here for the sake of brevity, are obtained for T_{ERA}).

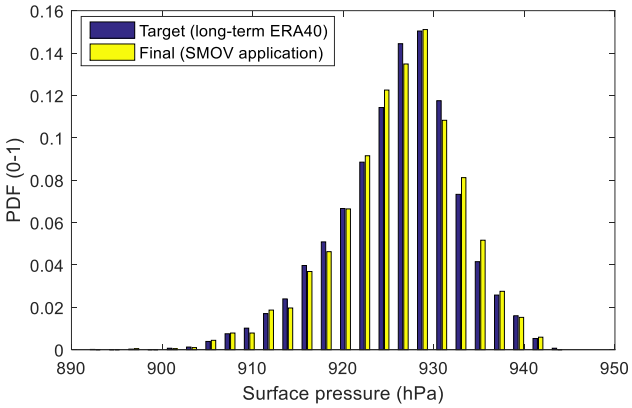

Fig. 7. PDF originating from 5 years of P_{ERA} values extracted from the ERA40 database (the reference site is Spino d'Adda), as well as from the same values characterizing all the water vapor fields generated by SMOV.

IV. Combination of all constituents: summary workflow

Based on the discussion above, Fig. 8 offers a summary of the whole procedure for the generation of correlated synthetic fields of rain rate, clouds and water vapor.

The workflow addresses the case in which all three constituents are simultaneously present, while, as mentioned above, rain-free cloud fields and clear sky water vapor fields are synthesized with no constraints on the choice of the (f_{ERA}, L_{ERA}) couple and of V_{ERA}, respectively, other than preserving the respective ERA40-derived PDFs. It is worth pointing out that, as clarified in the workflow, M_t and the other ERA40 derived quantities do not necessarily refer to the same 6-hour slot, while time concurrency is imposed for f_{ERA}, L_{ERA}, V_{ERA}, P_{ERA}, T_{ERA}, which are all selected from the same slot to preserve their high-level correlation.

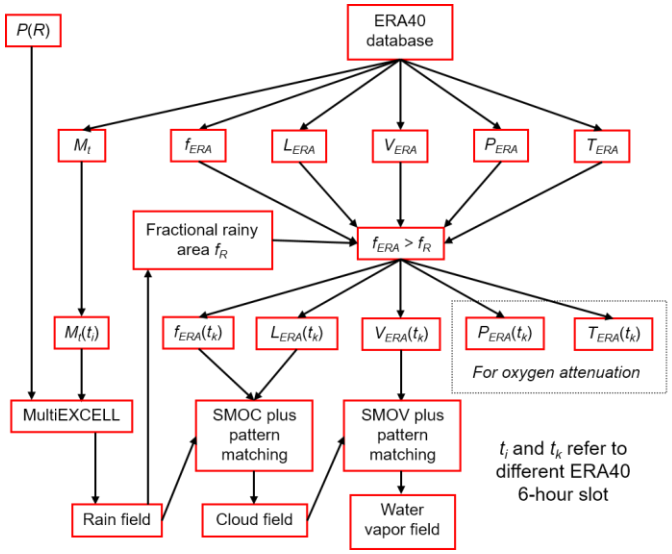

Fig. 8. Summary workflow for the generation of correlated synthetic fields of rain rate, clouds and water vapor.

V. Calculation of Attenuation

The total attenuation affecting Earth-space communication systems can be estimated using ATM PROP by simulating the interaction of the full tropospheric environment with the reference system. In general, the path attenuation along an Earth-space link is given by:

$$A^j = \int_{L_S} \gamma^j(l)\, dl \quad \text{(dB)} \tag{2}$$

where L_S is the portion of the slant link affected by a constituent j (e.g. rain, clouds, water vapor), whose specific attenuation γ_j is a function of the position l along the path. When applied to the synthetic maps of precipitation, clouds and water vapor, equation (2) is discretized. As for rain attenuation, it becomes:

$$A^R = \sum_{i=1}^{N} \gamma_i^R \, \Delta l_i = \sum_{i=1}^{N} k(R_i)^{\alpha} \, \Delta l_i \quad \text{(dB)} \tag{3}$$

where N is the total number of voxels crossed by the considered link, each of which is indexed by i, Δl_i is the portion of the link crossing the i-th voxel (as mentioned, its horizontal dimension is 1 km×1 km and its vertical extent is 100 m), R_i is the rain rate (mm/h) associated to voxel i, while k and α are the power-law coefficients extracted from recommendation ITU-R P.838-3 [26] as a function of frequency, link elevation and wave polarization. The number of total pixels N involved in (3) will depend on the local stratiform and convective rain heights.

As for the effects induced by clouds and water vapor, the attenuation due to the former (A^L) and to the latter (A^V) is calculated by exploiting the concept of mass absorption coefficient, as reported in [27] and [28], respectively. This approach avoids the need of additional information to calculate A^L and A^V, i.e. the knowledge of the vertical distribution of P and T, as such information is already embedded in the mass absorption coefficient. Thus, for A^L and A^V equation (2) turns into:

$$A^L = a_W \sum_{i=1}^{N} w_i \, \Delta l_i = a_W \, W_P \quad \text{(dB)} \tag{4}$$

$$A^V = a_V \sum_{i=1}^{N} v_i \, \Delta l_i = a_V \, V_P \quad \text{(dB)} \tag{5}$$

In (4), w_i is the liquid water content (g/m^3) in voxel i, W_P is the total liquid water content integrated along the path (mm) and a_W is the liquid water mass absorption coefficient − function of frequency − given by (8) in [27]. Similarly, in (5), v_i is the water vapor content (g/m^3) in voxel i, V_P is the total water vapor content integrated along the path (mm) and a_V is the water vapor mass absorption coefficient − function of frequency, ground station altitude and V − given by (7) in [28]. As a matter of fact, the applicability of ATM PROP to predict tropospheric attenuation is currently limited by this latter equation, which, as reported in [28], is valid between 20 and 100 GHz. However, such limits are planned to be overcome in the near future by extending the validity of both (4) and (5) to the full 1-350 GHz range.

Finally, as anticipated in Section III.B, the attenuation due to oxygen is calculated using equation (1), where, in turn, the zenithal attenuation due to oxygen A_Z^{OX} is estimated according to the procedure in Annex 2 of recommendation ITU-R P.676-10 [25], using as input P_{ERA} and T_{ERA}.

In order to improve the statistical significance of the attenuation predictions obtained by means of ATM PROP, equations (3), (4) and (5) can be repeatedly applied for every position of the ground station across the whole maps. As a result, full attenuation maps are obtained, which thoroughly take into account the possible interaction between the link and the surrounding atmospheric environment.

A key advantage of ATM PROP is offered by the chance to combine the contributions due to precipitation, clouds and gases on an "instantaneous basis", rather than on a statistical basis, as currently recommended in ITU-R P.618-12 [29]: indeed the latter approach addresses a "worst-case" scenario, as the various contributions to attenuation are summed up on equiprobable basis. On the other hand, the approach used in ATM PROP is expected to provide an increased prediction accuracy, because the rain rate, cloud and water vapor fields are combined so as to maintain a more realistic mutual correlation. Furthermore, an additional advantage offered by ATM PROP is the chance to take into due account the Earth's curvature, as well as the ray bending due to the variation of the refractive index n with height h. Specifically, such effects, more and more marked as the link elevation angle decreases to very low values (e.g. below 10°), are taken into account in ATM PROP using the calculation approach included in Section 2.2 of recommendation ITU-R P.676-10 [25], and by assuming the standard atmospheric profile for which the gradient of the refractive index with height (close to the ground), dn/dh, is -40×10^{-6} km^{-1} [30].

As an example of the use of ATM PROP to predict total tropospheric attenuation, Fig. 9 depicts the attenuation due to rain, clouds and water vapor, as well as the total tropospheric attenuation obtained as the summation of the said components plus the contribution of oxygen (0.08 dB for the whole map). The characteristics of the reference Earth-space link used to

obtain the results in Fig. 9 are the following: frequency f = 20 GHz, link elevation θ = 40°, azimuth ϕ = 90°, vertical linear polarization.

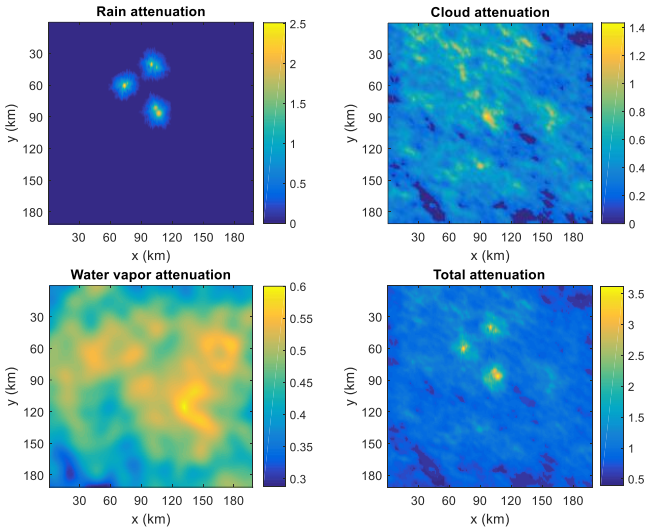

Fig. 9. Example of the use of ATM PROP to predict total tropospheric attenuation: separate contributions due to rain, clouds and water vapor, and total tropospheric attenuation (oxygen attenuation = 0.08 dB for the whole map).

VI. Validation of ATM PROP

The comprehensive validation of ATM PROP is not trivial as it consists of several elements, going from the preservation of the main features of precipitation, clouds and water vapor (i.e. first-order statistics and spatial correlation), to the combination of all the constituents in such a way to maintain their mutual correlation. A valuable chance for the validation of ATM PROP is offered by the large propagation dataset collected at the experimental station in Spino d'Adda, Italy, during the ITALSAT propagation campaign. Among all the data recorded for 7 years are the signal levels received from the three beacons onboard the ITALSAT satellite (frequency f = 18.7, 31.6 and 49.5 GHz; 37.7° link elevation, circular polarization for 31.6 GHz and linear for the other two frequencies), together with meteorological information coming from pressure, temperature and relative humidity sensors, as well as from a high-resolution tipping bucket raingauge (0.2 mm tip accumulation, time stamps with indication of the second). Radiometric data at 23.8 and 31.6 GHz were also collected to support the conversion of beacon signals into total tropospheric attenuation. Finally, as an additional source of data, high-resolution RAOBS were collected for 10 years (1980-1989) in Milano Linate airport, approximately 20 km from Spino d'Adda.

ATM PROP was applied to generate the full synthetic environment for the site of Spino d'Adda and the geometrical/electrical features mentioned above were used to calculate the atmospheric link attenuation at 18.7, 39.6 and 49.5 GHz. Concerning rain attenuation, the long-term $P(R)$ measured by the local raingauge collocated with the beacon receivers in Spino d'Adda was used as input to MultiEXCELL to synthesize rain maps, while the stratiform and convective rain heights are summarized in Table I. Concerning the attenuation due to clouds and gases, the necessary inputs to SMOC and SMOV were extracted from the ERA40 database, as shown in Fig. 8. In this specific case, 402 rain fields, 1995 cloud fields and 2032 water vapor fields were synthesized.

TABLE I. Stratiform and Convective Rain Height (km) Calculated for Spino d'Adda for the Two Frequencies.

	H_{str}	H_{cnv}
f = 39.6 GHz	3.99	3.69
f = 49.5 GHz	3.83	3.69

Fig. 10, Fig. 11 and Fig. 12 show the accuracy of ATM PROP in reproducing the atmospheric environment. Specifically, Fig. 10 compares the local $P(R)$ provided as input to MultiEXCELL with the statistics obtained from the whole set of synthetic rain maps; Fig. 11 and Fig. 12 refer to the CCDFs of integrated liquid water content (L) and integrated water vapor content (V), respectively, as calculated from the extensive RAOBS dataset mentioned above and as derived from all the cloud and water vapor maps synthesized by SMOC and SMOV, respectively. All the results clearly indicate a very good accuracy of ATM PROP in reproducing first-order statistics of the relevant atmospheric constituents.

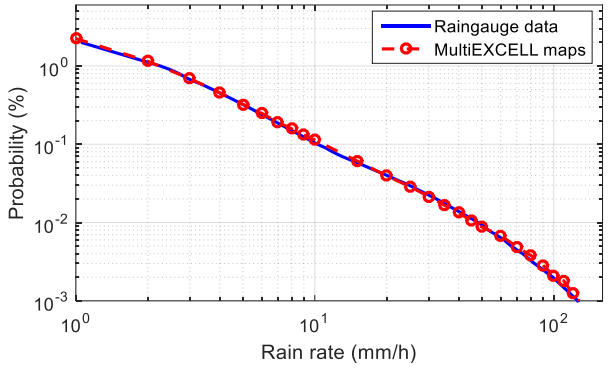

Fig. 10. Local $P(R)$ provided as input to MultiEXCELL (blue curve) and $P(R)$ obtained from the whole set of synthetic rain maps generated by MultiEXCELL (red curve). Site: Spino d'Adda.

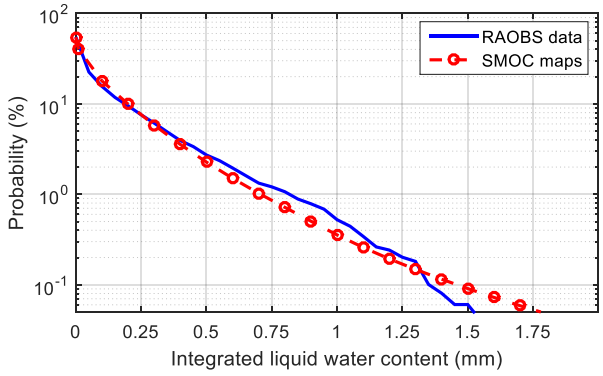

Fig. 11. Local statistics of integrated liquid water content L obtained from RAOBS data (blue curve) and from the whole set of synthetic cloud maps generated by SMOC (red curve). Site: Spino d'Adda.

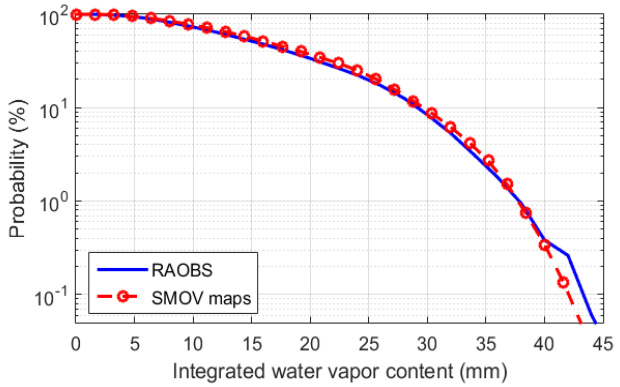

Fig. 12. Local statistics of integrated water vapor content V obtained from RAOBS data (blue curve) and from the whole set of synthetic water vapor maps generated by SMOV (red curve). Site: Spino d'Adda.

As an additional qualitative assessment of ATM PROP, Fig. 13 and Fig. 14 give a hint of how the model preserves the mutual spatial correlation between the three fields. Fig. 13 reports, for a sample rain field and its associated cloud field, the trend of the rain rate R and of the integrated liquid water content L as a function of y and for a fixed value of x (top side). Fig. 13 (bottom part) also depicts the vertical development of R (mm/h) and of the liquid water content (g/m^3), which shows that, as already mentioned, R is constant from the ground up to the rain height (fixed to 2.5 km in this case), where the cloud base lies, and that the downpour is associated to heavier clouds. Similarly, Fig. 14 depicts (top part), for the water vapor map associated to the cloud map, the trend of V with y (for the same x position), as well as spatial distribution of the water vapor content across the y/h plane (bottom part). As expected, the highest concentration of V corresponds to heavier clouds.

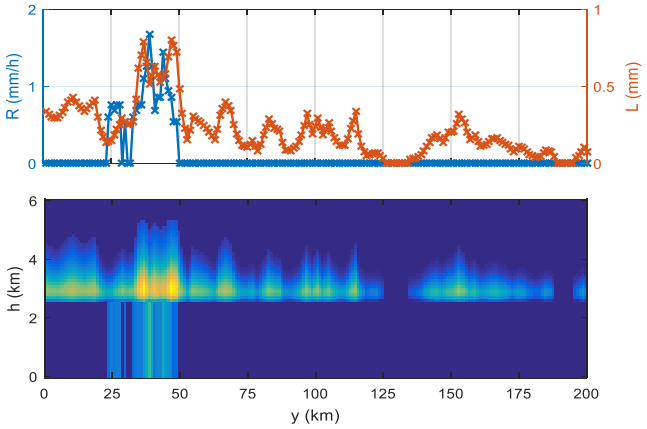

Fig. 13. Trend of R and L with y for a sample of coupled rain rate and cloud fields (top part), together with the vertical development of precipitation and clouds (bottom part).

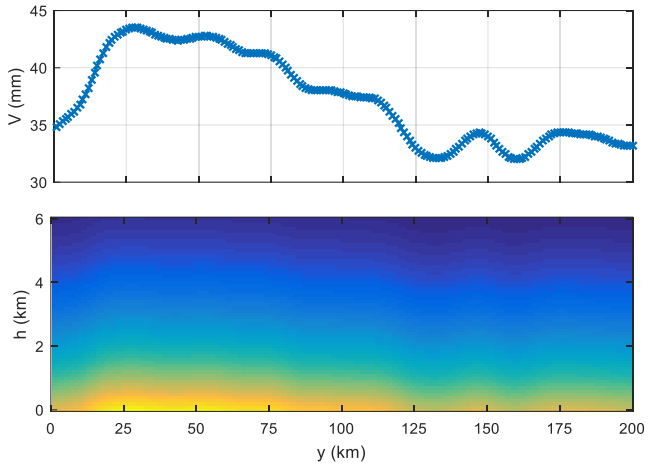

Fig. 14. Trend of V with y for the water field associated with the cloud field in Fig. 13 (top part), together with the vertical development of the water vapor content (bottom part).

Additional elements for the validation of ATM PROP comes from the beacon-derived attenuation data. Fig. 15 and Fig. 16 compare the long-term (7 years) mean yearly CCDF of the total attenuation (rain, clouds, water vapor and oxygen) for the two out of the three beacon frequencies (typically referred to as $P(A)$), together with the predictions delivered by ATM PROP, as well as by the combination of the methodologies recommended by ITU-R for electromagnetic propagation prediction along Earth-space links [29]: data for f = 18.7 GHz have been discarded because of the current limitations in applying ATM PROP to predict tropospheric attenuation (20-100 GHz range as explained in Section V).

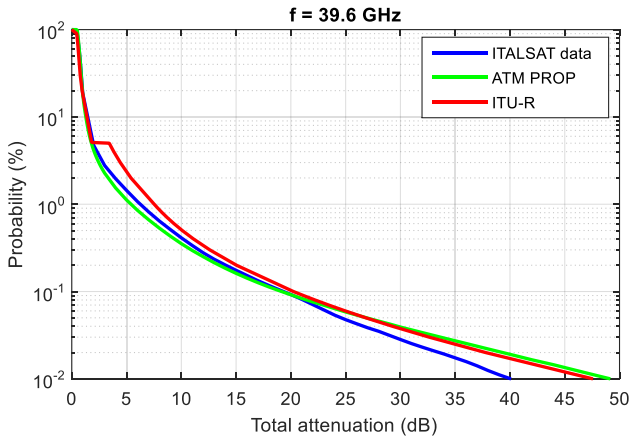

Fig. 15. Long-term (7 years) mean yearly CCDF of the total attenuation (ITALSAT experiment) at 39.6 GHz, together with the predictions delivered by ATM PROP and by the ITU-R approach.

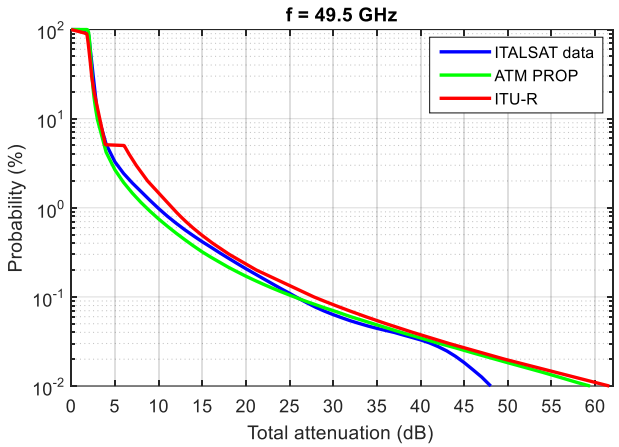

Fig. 16. Long-term (7 years) mean yearly CCDF of the total attenuation (ITALSAT experiment) at 49.5 GHz, together with the predictions delivered by ATM PROP and by the ITU-R approach.

In order to quantify the attenuation prediction accuracy of the two approaches, we have used the customary error figure $\psi_A(P)$ defined in recommendation ITU-R P.311-15 [31]:

$$\psi_A(P) = \begin{cases} \left(\frac{A_R(P)}{10}\right)^{0.2} & A_R(P) < 10 \text{ dB} \\ \ln\left(\frac{A_P(P)}{A_R(P)}\right) & A_R(P) \geq 10 \text{ dB} \end{cases} \quad (6)$$

In (6), $A_R(P)$ and $A_P(P)$ represent the path attenuations, both correspondent to probability level P, extracted respectively from the reference and the estimated $P(A)$. Table II lists the average (E) and root mean square (RMS) values of $\psi_A(P)$ for both frequencies and for the two models ($P \geq 10^{-2}$%). Both approaches provide quite a satisfactory prediction accuracy, which increases with frequency in both cases. The overestimation delivered by both models at 39.6 GHz and 49.5 GHz can be partially ascribed to the limited dynamics of the ITALSAT beacon receivers. ATM PROP shows a much better performance than the ITU-R model (RMS approximately halved): as is clear from Fig. 15 and Fig. 16, $P(A)$ curves predicted using the ITU-R approach are characterized by a sharp "jump" due both to the ITU-R rain attenuation prediction model and to the statistical approach for the combination of the various contributions to total attenuation [29].

TABLE II. AVERAGE (E) AND ROOT MEAN SQUARE (RMS) VALUES OF THE ESTIMATION ERROR FOR THE TWO FREQUENCIES AND THE TWO PREDICTION APPROACHES.

	***f* = 39.6 GHz**		***f* = 49.5 GHz**	
	E	**RMS**	**E**	**RMS**
ITU-R	0.088	0.184	0.110	0.177
ATM PROP	0.022	0.086	0.048	0.077

Though additional experimental data are required to more thoroughly validate ATM PROP, the results presented here are encouraging and suggest the use of ATM PROP in more complex scenarios (out of the scope of this paper, though) such as those involving low elevation links (e.g. LEO links or GEO links at high latitude) and/or systems distributed in space (e.g. site diversity schemes): indeed, in these cases, the spatial distribution of the relevant tropospheric constituents, as well as "secondary" effects such as ray bending, need to be taken in due account in order to provide more accurate predictions.

VII. CONCLUSIONS

This contribution presents ATM PROP (ATMospheric simulator for PROPagation applications), a comprehensive methodology aimed at predicting tropospheric effects affecting high-frequency Earth-space communication systems on areas as large as 200 km×200 km. The model combines three-dimension synthetic fields of rain rate, clouds and water vapor (1 km×1 km horizontal resolution, 100 m vertical detail from the ground up to 20 km) to reproduce the tropospheric environment impairing EM waves.

Precipitation and cloud fields, synthesized by MultiEXCELL and SMOC using as input coarse-resolution ERA40-derive meteorological inputs (2°×2° latitude/longitude grid), are merged by satisfying the obvious constraint that rainy areas are fully covered by clouds and, in addition, by imposing that precipitation is associated to heavier clouds. Water vapor fields, generated by SMOV using again inputs from the ERA40 database, are afterwards added to the environment by ensuring that clouds lie where the humidity is higher. Finally, the effect of oxygen is included by assuming that the associated path attenuation is constant across the considered area. As a result, the generated synthetic environment not only correctly reproduces first-order (CCDF) and second-order (spatial correlation) statistics of rain rate, clouds and water vapor, but also maintains their mutual correlation. This has been preliminary validated using as reference the large propagation dataset collected at the experimental station of Spino d'Adda during the ITALSAT campaign: the comparison against meteorological data (raingauge-derived R, RAOBS-derived L and V), as well as total tropospheric attenuation obtained from the ITALSAT beacons (f = 39.6 and 49.5 GHz) indicate a very satisfactory prediction accuracy delivered by ATM PROP. Though additional experimental data are needed to more thoroughly validate ATM PROP, these results are encouraging and suggest the use of ATM PROP in more complex scenarios such as those involving very low elevation links (e.g. LEO links or GEO links at high latitude) and/or systems distributed in space (e.g. site diversity schemes): indeed, in these cases, the spatial distribution of the relevant tropospheric constituents, and "secondary" effects such as ray bending, need to be taken in due account in order to provide more accurate predictions. These further applications of ATM PROP, as well as the activities to model the time evolution of the tropospheric environment (already initiated in [32] and [33]), are part of the future work.

ACKNOWLEDGMENT

This effort was sponsored by the Air Force Office of Scientific Research, Air Force Material Command, USAF, under grant number FA8655-13-1-3081. The U.S Government is authorized to reproduce and distribute reprints for Governmental purpose notwithstanding any copyright notation thereon. The authors would also like to acknowledge the ECMWF for granting access to the datasets included in the ERA40 database.

REFERENCES

[1] N. Jeannin, L. Castanet, J. Radzik, M. Bousquet, B. Evans, P. Thompson, "Smart gateways for terabit/s satellite," International Journal of Satellite Communications and Networking, vol. 32 (n° 2). pp. 93-106, 2014.

[2] EOARD Award FA8655-12-1-2062, "Performance evaluation of Satellite Communication systems operating in the Q/V/W band".

[3] C. Riva, C. Capsoni, L. Luini, M. Luccini, R. Nebuloni, A. Martellucci, "The Challenge of Using the W Band in Satellite Communication," Int. J. Satell. Commun. Network. 2014; 32:187–200.

[4] P. Arapoglou, A. D. Panagopoulos, "A tool for synthesizing rain attenuation time series in LEO Earth observation satellite downlinks at Ka band", EuCAP 2011, pp. 1467 – 1470, Prague, Czech Republic, 2011.

[5] J. E. Allnutt, "Satellite to Ground Radiowave Propagation," 2nd Edition, The Institution of Engineering and Technology, May 2010.

[6] ESA/ESTEC/Contract 17760/03/NL/JA, "Characterisation and modelling of propagation effects in 20-50 GHz band".

[7] L. Luini, C. Capsoni, "A Rain Cell Model for the Simulation and Performance Evaluation of Site Diversity Schemes," IEEE Antennas and Wireless Propagation Letters, vol. 12, No. 1, Page(s): 1327-1330, 2013.

[8] L. Luini, C. Capsoni, "MultiEXCELL: a new rain field model for propagation applications," IEEE Transactions on Antennas and Propagation, vol. 59, no. 11, Page(s): 4286 – 4300, November 2011.

[9] L. Feral, H. Sauvageot, L. Castanet, J. Lemorton, "HYCELL-A new hybrid model of the rain horizontal distribution for propagation studies: 2. Statistical modeling of the rain rate field", Radio Science, Vol. 38, No. 3, 2003.

[10] C. I. Kourogiorgas, G. A. Karagiannis, A. D. Panagopoulos, "Space-time rain rate field generator for multi-antenna satellite communication applications," 7th European Conference on Antennas and Propagation (EuCAP), pp. 42-45, 8-12 April, 2013, Göteborgh, Sweden.

[11] N. Jeannin, L. Féral, H. Sauvageot, L. Castanet, F. Lacoste: "A large-scale space-time stochastic simulation tool of rain attenuation for the design and optimization of adaptive satellite communication systems operating between 10 and 50 GHz," International Journal of Antennas and Propagation, Volume 2012 (2012), Article ID 749829, 16 pages.

[12] B.C. Gremont, F. Filip, "Spatio-temporal rain attenuation model for application to fade mitigation techniques," IEEE Trans. Ant. and Prop., Vol. 52, No. 5, May, 2004.

[13] L. Luini, C. Capsoni, "Modeling High Resolution 3-D Cloud Fields for Earth-space Communication Systems," IEEE Transactions on Antennas and Propagation, vol. 62, no. 10, Page(s): 5190 - 5199, October 2014.

[14] N. K. Lyras, C. I. Kourogiorgas, A. D. Panagopoulos, "Cloud Attenuation Statistics Prediction From Ka-Band to Optical Frequencies: Integrated Liquid Water Content Field Synthesizer," IEEE Transactions on Antennas and Propagation, vol. 65, no. 1, Page(s): 319 – 328, January 2017.

[15] L. Luini, "Modeling and Synthesis of 3-D Water Vapor Fields for EM Wave Propagation Applications," IEEE Transactions on Antennas and Propagation, vol. 64, no. 9, Page(s): 3972 - 3980, September 2016.

[16] A. J. Page,R. J. Watson, P. A. Watson, "Time-series of attenuation on EHF and SHF fixed radio links derived from meteorological forecast and radar data," IEE Proceedings - Microwaves, Antennas and Propagation, Volume: 152, Issue: 2, pp. 124–128, Apr. 2005.

[17] M. O. García, N. Jeannin, L. Féral, L. Castanet, "Use of WRF model to characterize propagation effects in the troposphere," 7th European Conference on Antennas and Propagation (EuCAP), pp. 1377-1381, 8-12 April, 2013, Göteborg, Sweden.

[18] S. M. Uppala, P. W. Kallberg, et al., "The ERA-40 Re-analysis," Quart. J. Roy. Meteor. Soc., 131, pp. 2961-3012, 2005.

[19] C. Capsoni, L. Luini, M. D'Amico, "The MultiEXCELL model for the prediction of the radio interference due to hydrometeor scattering," 4th European Conference on Antennas and Propagation (EuCAP), pp. 1-5, 12-16 April 2010, Barcelona, Spain

[20] L. Luini, L. Emiliani, C. Capsoni "Planning of Advanced SatCom Systems Using ACM Techniques: The Impact of Rain Fade," 5th European Conference on Antennas and Propagation (EuCAP), pp. 3965-3969, 11-15 April 2011, Rome, Italy.

[21] C. Capsoni, L. Luini, A. Paraboni, C. Riva, "Stratiform and convective rain discrimination deduced from local $P(R)$," IEEE Transactions on Antennas and Propagation, vol. 54, issue 11, pp. 3566-3569, Nov. 2006.

[22] C. Capsoni, L. Luini, A. Paraboni, C. Riva, A. Martellucci, "A new prediction model of rain attenuation that separately accounts for stratiform and convective rain," IEEE Transactions on Antennas and Propagation, Vol 57, No. 1, pp. 196-204, January, 2009.

[23] T. L. Bell, "A Space-Time Stochastic Model of Rainfall for Satellite Remote-Sensing Studies," Journal of Geophysical Research, Vol. 92, No. D8, pp. 9631-9643, 1987.

[24] C. Capsoni, L. Luini, "The SC EXCELL Model for the Prediction of Monthly Rain Attenuation Statistics," pp. 1382-1385, EuCAP 2013, 8-12 April 2013, Goteborg, Sweden.

[25] Attenuation by atmospheric gases. Geneva, 2013, ITU-R recommendation P.676-10.

[26] Specific attenuation model for rain for use in prediction methods. Geneva, 2005, ITU-R recommendation P.838-3.

[27] L. Luini, C. Capsoni, "Efficient Calculation of Cloud Attenuation for Earth-space Applications," IEEE Antennas and Wireless Propagation Letters, vol. 13, pp. 1136-1139, 2014.

[28] L. Luini, C. Riva, "Improving the Accuracy in Predicting Water Vapor Attenuation at Millimeter-wave for Earth-space Applications," IEEE Transactions on Antennas and Propagation, vol. 64, no. 6, pp. 2487-2493, June 2016.

[29] Propagation data and prediction methods required for the design of Earth-space telecommunication systems. Geneva, 2015, ITU-R recommendation P.618-12.

[30] Prediction procedure for the evaluation of interference between stations on the surface of the Earth at frequencies above about 0.1 GHz. Geneva, 2015, ITU-R recommendation P.452-16.

[31] Acquisition, presentation and analysis of data in studies of tropospheric propagation. Geneva, 2015, ITU-R recommendation P.311-15.

[32] C. Capsoni, L. Luini, "Analysis of the spatial and temporal properties of rain cells for rainfall modeling purposes," Italian Journal of Remote Sensing, 2009, 41 (3): 51-62.

[33] S. Ghirardin, C. Capsoni, L. Luini, "Time Evolution of Synthetic Rain Cells for the Synthesis of Attenuation Time Series," 10th European Conference on Antennas and Propagation (EuCAP), 10-15 April 2016, pp. 1-5, Davos, Switzerland.